

A low-noise X-band microwave source with digital automatic frequency control for electron paramagnetic resonance spectroscopy

Yu He(贺羽), Runqi Kang(康润琪), Zhifu Shi(石致富), and Xing Rong(荣星)
Citation: Chin. Phys. B, 2023, 32 (**8**): 087601. DOI: 10.1088/1674-1056/accf7e
Journal homepage: http://cpb.iphy.ac.cn; http://iopscience.iop.org/cpb

What follows is a list of articles you may be interested in

A design of resonant cavity with an improved coupling-adjusting mechanism for the W-band EPR spectrometer

Yu He(贺羽), Runqi Kang(康润琪), Zhifu Shi(石致富), Xing Rong(荣星), and Jiangfeng Du(杜江峰)
Chin. Phys. B, 2022, 31 (**11**): 117601. DOI: 10.1088/1674-1056/ac7bfd

Determination of charge-compensated C_{3v} (II) centers for Er^{3+} ions in CdF_2 and CaF_2 crystals

Rui-Peng Chai(柴瑞鹏), Dan-Hui Hao(郝丹辉), Dang-Li Gao(高当丽), and Qing Pang(庞庆)
Chin. Phys. B, 2021, 30 (**3**): 037601. DOI: 10.1088/1674-1056/abc3b0

Covalent bonding and *J-J* mixing effects on the EPR parameters of Er^{3+} ions in GaN crystal

Rui-Peng Chai(柴瑞鹏), Long Li(李隆), Liang Liang(梁良), Qing Pang(庞庆)
Chin. Phys. B, 2016, 25 (**7**): 077601. DOI: 10.1088/1674-1056/25/7/077601

An electron spin resonance study of Eu doping effect in $La_{4/3}Sr_{5/3}Mn_2O_7$ single crystal

He Li-Min (何利民), Ji Yu (冀钰), Wu Hong-Ye (吴鸿业), Xu Bao (徐宝), Sun Yun-Bin (孙运斌), Zhang Xue-Feng (张雪峰), Lu Yi (鲁毅), Zhao Jian-Jun (赵建军)
Chin. Phys. B, 2014, 23 (**7**): 077601. DOI: 10.1088/1674-1056/23/7/077601

Abnormal magnetic behaviors induced by the antisite phase boundary in La_2NiMnO_6

Zhao Yue-Lei (赵月雷), Chai Yi-Sheng (柴一晟), Pan Li-Qing (潘礼庆), Sun Young (孙阳)
Chin. Phys. B, 2013, 22 (**8**): 087601. DOI: 10.1088/1674-1056/22/8/087601

INSTRUMENTATION AND MEASUREMENT

A low-noise X-band microwave source with digital automatic frequency control for electron paramagnetic resonance spectroscopy

Yu He(贺羽)[1,2], Runqi Kang(康润琪)[1,2], Zhifu Shi(石致富)[3], and Xing Rong(荣星)[1,2,4,†]

[1] *CAS Key Laboratory of Microscale Magnetic Resonance and School of Physical Sciences, University of Science and Technology of China, Hefei* 230026, *China*

[2] *CAS Center for Excellence in Quantum Information and Quantum Physics, University of Science and Technology of China, Hefei* 230026, *China*

[3] *Chinainstru & Quantumtech (Hefei) Co., Ltd, Hefei* 230031, *China*

[4] *Hefei National Laboratory, University of Science and Technology of China, Hefei* 230088, *China*

(Received 24 February 2023; revised manuscript received 18 April 2023; accepted manuscript online 24 April 2023)

We report a new design of microwave source for X-band electron paramagnetic resonance spectrometer. The microwave source is equipped with a digital automatic frequency control circuit. The parameters of the digital automatic frequency control circuit can be flexibly configured for different experimental conditions, such as the input powers or the quality factors of the resonator. The configurability makes the microwave source universally compatible and greatly extends its application. To demonstrate the ability of adapting to various experimental conditions, the microwave source is tested by varying the input powers and the quality factors of the resonator. A satisfactory phase noise as low as −135 dBc/Hz at 100-kHz offset from the center frequency is achieved, due to the use of a phase-locked dielectric resonator oscillator and a direct digital synthesizer. Continuous-wave electron paramagnetic resonance experiments are conducted to examine the performance of the microwave source. The outstanding performance shows a prospect of wide applications of the microwave source in numerous fields of science.

Keywords: electron paramagnetic resonance, X-band, microwave source, automatic frequency control

PACS: 76.30.–v, 33.35.+r, 07.57.–c, 84.40.–x **DOI:** 10.1088/1674-1056/accf7e

1. Introduction

Electron paramagnetic resonance (EPR) is a significant spectroscopic technology that investigates materials with unpaired electrons.[1–3] The energy levels of electrons in the sample split in a magnetic field. When the microwave (mw) frequency matches the splitting, resonant absorption occurs. The imaginary part of the magnetic susceptibility χ $(=\chi'+\mathrm{i}\chi'')$ results in a dip of the reflected mw power. EPR is broadly applied in many fields of natural sciences and medicine.[4–8] Up to now, the EPR technology of X-band is the maturest and most widely used, because of the boom of X-band mw technology and the limit of magnetic field generated by electromagnets.

The mw source is a crucial component of an EPR spectrometer. It provides mw of a specific frequency that is delivered to and interacts with the sample. Klystrons and Gunn diodes are widely used as mw sources in EPR.[9–11] Tuning of their output frequency can be done both manually and automatically.[9,12,13] The manual tuning is realized by varying the size of the tuning cavity. By the manual method, the output frequency can vary in the range of several gigahertz. On the other hand, the automatic tuning can be realized by changing the bias voltage, but the tuning range of the automatic method is limited to tens of megahertz. In continuous-wave (cw) EPR experiments, the mw frequency is required to match the resonant frequency of the resonant cavity for perfect impedance matching and maximized sensitivity. However, many factors may change the resonant frequency of the cavity in practice, such as changes in the real part of the magnetic susceptibility, the heating effect of the input mw and the thermal expansion or contraction caused by the variable temperature system.[14] The deviation between the input frequency and the resonant frequency mixes the absorption term (χ'') and the dispersion term (χ') and degrades the performance of the EPR signal: it deforms the line shape of the spectra, increases noises and causes baseline drifts.[15]

In order to cancel the negative influences of the variation of the resonant frequency, automatic frequency control (AFC) is utilized in mw sources for EPR.[15–19] The main idea of AFC is to modulate the frequency of the mw and extract the error signal by demodulation. Microwave sources with AFCs automatically and simultaneously track the resonant frequency of the cavity. As a result, the quality of the EPR spectra can be greatly improved. The most widely used mw sources, such as Gunn diodes and klystrons, are analog devices. Their output frequencies are controlled by the voltage. Meanwhile, there had been a lack of digital mw sources for a long time. Therefore, most of AFC designs are based on analog circuits. Since the electronic elements are fixed, the parameters of these AFC circuits can hardly be flexibly configured depending on the ex-

†Corresponding author. E-mail: xrong@ustc.edu.cn

© 2023 Chinese Physical Society and IOP Publishing Ltd

perimental conditions, such as the quality factor of the cavity or the input power of the mw. The continuous trend of improvement of performance and reliability of digital electronics promotes the study on digital AFCs. Efforts have also been made to develop AFCs that are based partially or completely on digital circuits. However, existing digital AFC circuits or algorithms mainly focus on applications in wireless radio communication systems,[20–22] while digital AFCs are rarely used and in high demand in the field of EPR.

Here we report an X-band mw source with a digital AFC integrated. The digital AFC overcomes the disadvantages of its analog counterparts. Configurability of our AFC is demonstrated by tests with cavities of different Q factors and under different mw powers. The mw source also shows outstanding performance in the test of phase noise. Continuous-wave EPR experiments have also been carried out to verify the performance of the mw source.

2. Design

The mw source should fulfill the requirement that the output frequency can vary from 9.2 GHz to 9.7 GHz, with a minimum step of 1 kHz. The phase noise should reach the typical level of an X-band mw source, i.e., −124 dBc/Hz at 100-kHz offset from the central frequency.[23] For these two reasons, a self-made phase-locked dielectric resonator oscillator (PDRO) and a direct digital synthesizer (DDS) are utilized to generate the mw. In addition, a microcontroller is employed to achieve a parameter-adjustable AFC. The adjustable ranges and steps of the AFC parameters are listed in Table 1.

Table 1. Adjustable ranges and steps of the AFC parameters.

Parameter	Range	Step
Modulation depth	0–100 kHz	10 kHz
P	0–20000	0.001
I	0–20000 rad/s	0.001 rad/s
D	0–20000 s/rad	0.001 s/rad
Lock-in time constant	1–1000 ms	10 ms

Figure 1 displays the block diagram of the mw source. The green, blue and red boxes represent the frequency mixing (FM) module, the direct digital synthesizer (DDS) and the AFC circuit, respectively. The DDS is developed based on AD9914 produced by Analog Devices, Inc., while the AFC is developed based on STM32F405RGT6 produced by STMicroelectronics. There are two operation modes in the mw source, which are AFC-off and AFC-on.

The FM module and the DDS are employed in the AFC-off mode, where the mw source outputs mw of a specific frequency. The output frequency of the PDRO is exactly 9 GHz, while the DDS outputs a signal of a specific pre-set frequency in the range of 200 MHz–900 MHz (bias frequency). These two arms of signals are up-converted in a mixer (Analog Devices, Inc., HMC787), forming a 9.2–9.9-GHz X-band microwave. The synthesized mw signal passes a band-pass filter (BPF, self-made) and a low-noise amplifier (LNA, Analog Devices, Inc., HMC3653) and is then fed into the mw bridge.

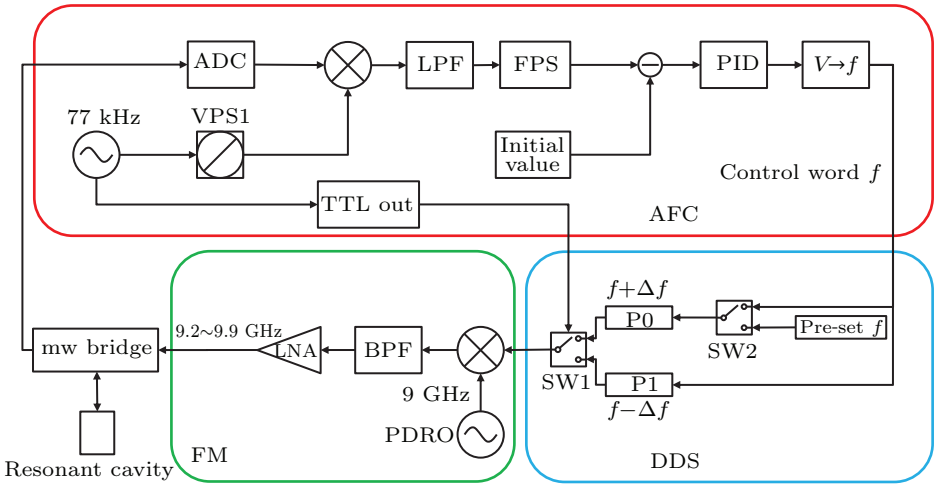


Fig. 1. Schematic diagram of the mw source. An FM module, a DDS and an AFC circuit are included. The AFC circuit receives a portion of the signal from the mw bridge, calculates the deviation of the mw frequency and sends the corrected offset frequency to the DDS. The bias signal is converted into a biased square wave in the DDS, and mixed with the signals of the local oscillation frequency in the FM module. Consequently, the mw source outputs mw ranging from 9.2 GHz to 9.9 GHz to the mw bridge, and the exact mw frequency keeps the same as the resonant frequency of the cavity.

In the AFC-on mode, another oscillator provides a 77-kHz cosine signal for frequency modulation. The modulation signal is then converted to a square wave and used as the trigger of the single-pole-double-throw switch (SW1). In the meantime, the values of the two profiles (P0 and P1) in the DDS are set to $f_0 = f + \Delta f$ and $f_1 = f - \Delta f$, where Δf is the modulation amplitude and f is the bias frequency. As a result, the output of the mw source periodically jumps between f_0 and f_1.

For simplicity, we merely consider the zero and first-

order expansion of the modulated signal, whose frequency is $f^{(1)} = 9\,\text{GHz} + f + \Delta f \cos(2\pi f_\text{m} t)$, where f_m is the modulation frequency, 77 kHz. When the resonant frequency f_c of the cavity deviates from $f + 9$ GHz, the output voltage signal of the detector diode in the mw bridge is a mixture of components at f_m and $2f_\text{m}$, with amplitudes V_1 and V_2, respectively. The output of the diode passes an analog-to-digital converter (ADC) and a mixer when fed into the AFC circuit. After mixed with the 77-kHz signal, the demodulated signal is low-pass filtered by a low pass filter (LPF). Consequently, only the amplitude of the f_m component, which contains the information of the frequency deviation, is retained as the correction signal, while the $2f_\text{m}$ component is discarded. It is worth mentioning that the variable phase shifter (VPS1) after the 77-kHz oscillator is used for the maximization of the DC correction signal, while the fixed phase shifter (FPS) after the LPF compensates the effect of another FPS of the mw bridge in the pulsed mode, ensuring the proper polarity of the correction signal.[24] The correction signal is subtracted from the initial offset voltage, coupled to a proportional–integral–derivative controller (PID) and converted to frequency control words. The bias frequency f in P0 and P1 are updated according to the control words. Therefore, the output frequency of the mw source, $f + 9$ GHz, is always locked to f_c.

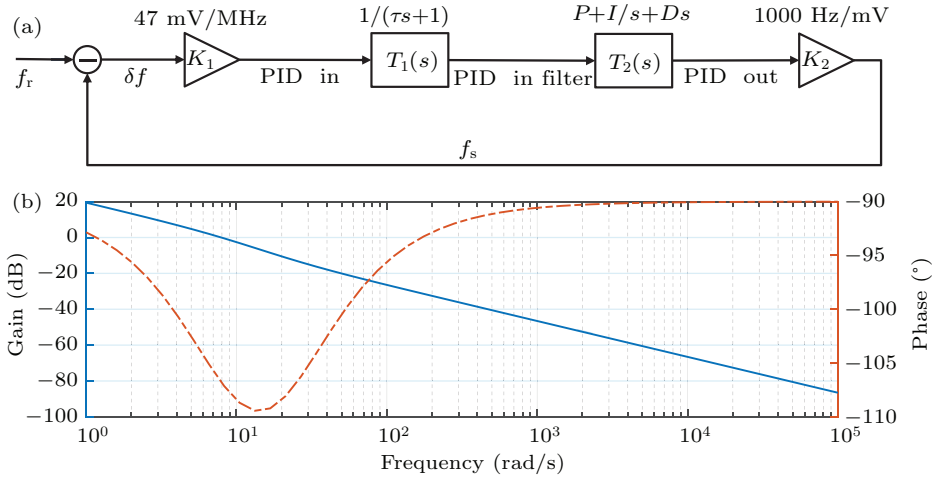


Fig. 2. (a) Schematic diagram of the AFC feedback loop. (b) A typical Bode plot of the open-loop transfer function of the AFC circuit. The parameters are set to $\tau = 0.1$ s, $P = 10$, $I = 200$ and $D = 0$. The resulting phase margin is 83°.

Figure 2(a) shows the feedback loop of the mw source. K_1 refers to the transformation coefficient from the error signal to the voltage. It depends on the mw power, the modulation depth and the quality factor of the cavity. K_1 is experimentally measured to be 47 mV/MHz in our tests. $T_1(s)$ is the transfer functions of the lock-in amplifier. It is in the $1/(\tau s + 1)$ form, where τ is the time constant that can be set manually, and s is the corresponding variable of time after the Laplace transformation. The PID transfer function is expressed as $T_2(s) = P + I/s + Ds$, where P, I and D are the proportional, integral and derivative terms, respectively. They are also configurable parameters. K_2 is the transformation coefficient from the output voltage of PID to the frequency, which is set as 1000 Hz/mV in our experiments. As a result, the total open-loop gain is

$$G_\text{open} = K_1 \times T_1(s) \times T_2(s) \times K_2. \tag{1}$$

Information of the phase margin can be extracted from the Bode plot of the open-loop gain. The phase margin is an indicator of the stability of the AFC. It is defined as the phase lag φ, where the open-loop gain of the circuit reaches 0 dB, minus $-180°$. Generally, a system is stable when the phase margin is larger than 45°. Here we take $\tau = 0.1$ s, $P = 10$, $I = 200$ and $D = 0$ for example. The Bode plot of our AFC circuit is shown in Fig. 2(b). It proves that our mw source is adequately stable with an outstanding phase margin of 83°.

3. Experimental setup

The mw source is installed in an X-band EPR spectrometer and a series of experiments have been conducted. The structure of the spectrometer is shown in Fig. 3.

Two arms are included in the mw bridge, the sample arm and the reference arm. The function of the attenuator in the sample arm (Att.1) is to adjust the mw power that is fed into the resonator. Since the detector is very fragile, a limiter (Ltr.) is used so that the power of EPR signal from the resonator cannot exceed a certain level. Then the EPR signal is amplified by LNA3 and detected by the detector diode (Det.). In order to ensure the unidirectional transmission of the mw and protect the front-end electronics from the reflected mw energy, a circulator (Cir.) is used. Another portion of the mw energy is tapped off into the reference arm, serving as a bias. The attenuator in the reference arm (Att.2) controls the mw power and ensures that the detector works in the linear zone. The VPS2 is utilized to compensate the phase difference between the two arms. A fraction of the output signal from the detector

is received by the mw source as feedback.

An electromagnet is used to generate an external magnetic field. Real-time monitoring of the magnetic field is achieved by a Hall sensor for stabilization of the magnetic field. In order to suppress the pink noise, the strength of the magnetic field is modulated sinusoidally using a pair of modulation coils.[25] The small-amplitude sinusoidal modulation signal is generated by a lock-in amplifier and a coil driver. As a result, the EPR signal is also modulated with the same frequency as the magnetic field. In field-swept EPR experiments, at each point of the central magnetic field, the magnetic field controller sends a trigger to the lock-in amplifier, then the lock-in amplifier starts collecting data. The lock-in amplifier demodulates the EPR signal and outputs the first-order derivative spectrum to the computer for further processing.

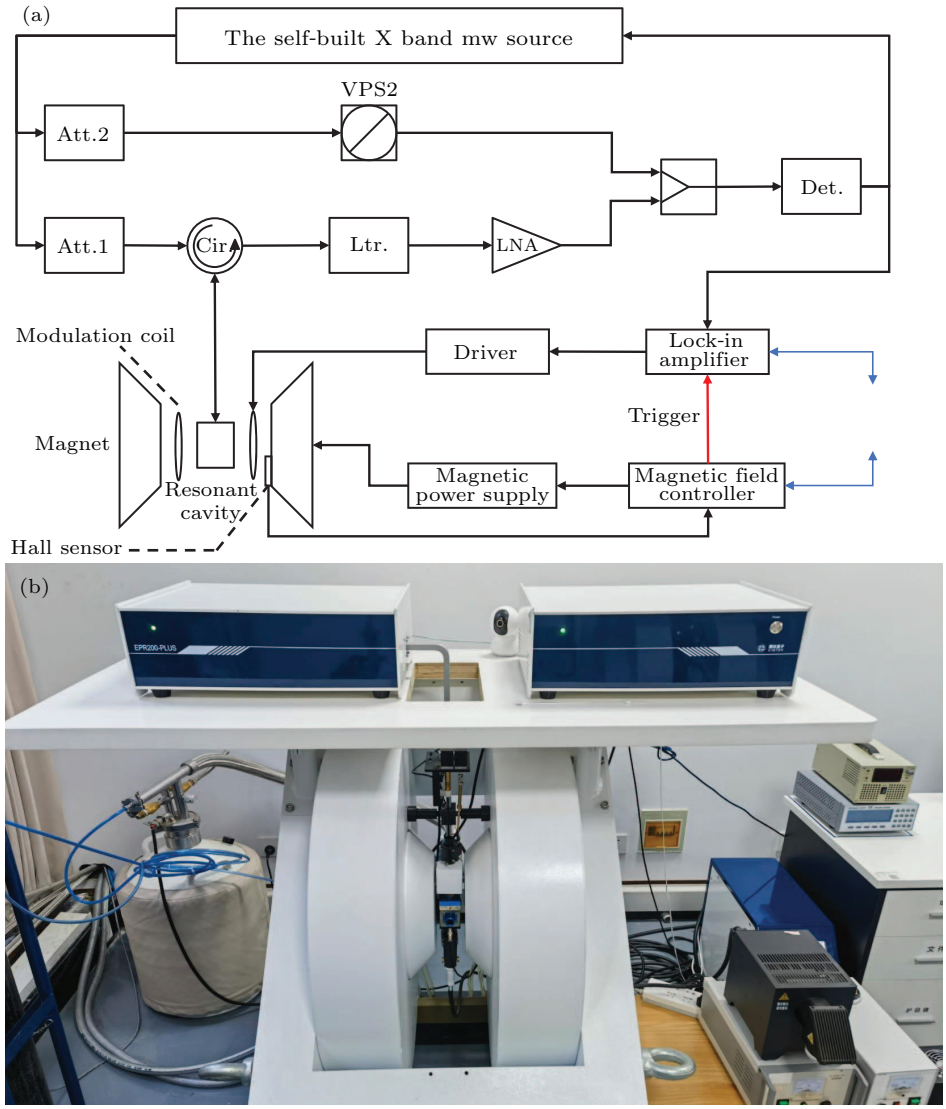


Fig. 3. (a) Schematic diagram of the X-band EPR spectrometer. The mw bridge consists of a sample arm and a reference arm. Signals from the two arms are combined and sensed by a detector diode. A portion of the output signal from the detector is sent to the mw source as feedback, while others are collected by the lock-in amplifier. An electromagnet and a pair of coils are used to provide the external magnetic field and the modulation field, respectively. The lock-in amplifier generates the modulation signal, demodulates the EPR signal and sends the data to the computer. (b) Photograph of the X-band EPR spectrometer.

4. Performance

4.1. Step response

To demonstrate the ability of AFC parameters to be flexibly configured according to experimental conditions, step responses with different resonant cavities and under different input powers were tested. Step response is the time-domain behavior of the output frequency of the mw source when there is a sudden change of the resonant frequency. It directly reveals the frequency-tracking ability of the AFC. By adjusting parameters in our digital AFC, the step responses can maintain optimized performances in different conditions. On the contrary, step responses of analog AFCs usually degrade when experimental conditions change, since their electronic elements are fixed.

Three groups of experiments were carried out, and the

results are shown in Fig. 4. The testing conditions were $Q = 3230$ and $P_{mw} = 0.1$ mW for group 1 [Fig. 4(a)], $Q = 3230$ and $P_{mw} = 100$ mW for group 2 [Fig. 4(b)] and $Q = 9000$ and $P_{mw} = 0.1$ mW for group 3 [Fig. 4(c)], where Q is the quality factor of the cavity and P_{mw} is the power of the input mw. In the first group of tests, we set the modulation depth Δf as 6 kHz, the time constant $\tau = 100$ ms, the proportional term $P = 10$ and the derivative term $D = 0$, and tried three values of I. Step responses when $I = 100$ rad/s, 200 rad/s and 500 rad/s are plotted as the blue solid line, the coral dash-dot line and the yellow dashed line. It is apparent that the step response is optimized when $I = 200$ rad/s, since the system responses fastest to the change of the resonant frequency and no undesirable oscillation is observed. In the second and the third group of tests, however, the best performances are obtained with the modulation depth being 150 Hz and 2 kHz, respectively. Additionally, the best choice of I becomes 100 rad/s rather than 200 rad/s. These tests show that the parameters of our AFC are configurable.

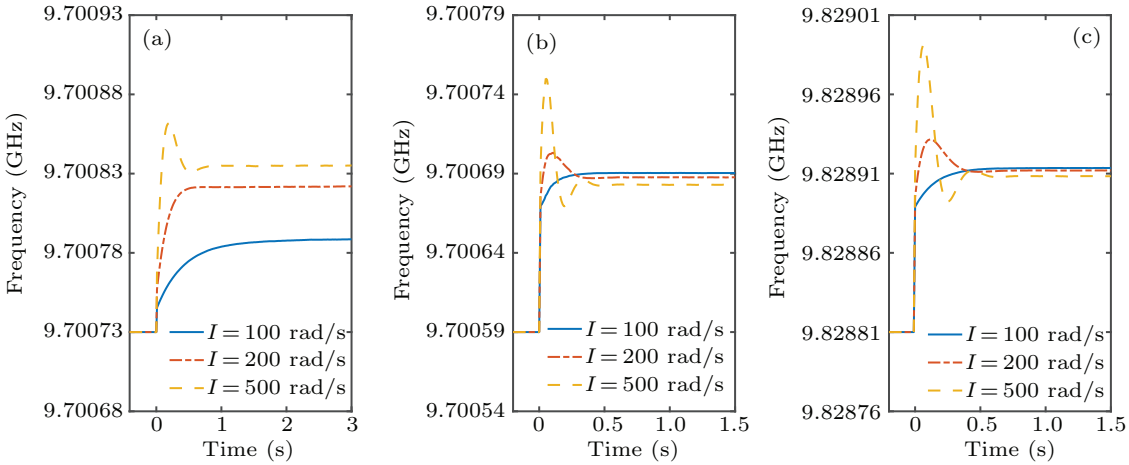


Fig. 4. Step responses obtained under different testing conditions and with different AFC configurations. In all of the three groups of tests, the time constant is set to 100 ms, the proportional term is set to 10 and the derivative term is set to 0. Experimental results with the integral term being 100 rad/s, 200 rad/s and 500 rad/s are plotted as the blue solid line, the coral dash-dot line and the yellow dashed line, respectively. (a) Step responses obtained with $Q = 3230$ and $P_{mw} = 0.1$ mW. The modulation depth is set to 6 kHz. (b) Step responses obtained with $Q = 3230$ and $P_{mw} = 100$ mW. The modulation depth is set to 150 Hz. (c) Step responses obtained with $Q = 9000$ and $P_{mw} = 0.1$ mW. The modulation depth is set to 2 kHz.

4.2. Phase noise

Phase noise represents the instability of a mw source. It causes variation of the central frequency and degrades the quality of EPR spectra.[26,27] Therefore, low phase noise is preferred in practice. The phase noise of the mw source offset from the center frequency of 9.7 GHz was measured using a phase noise analyzer (Rohde & Schwarz, FSW26). Figure 5 shows the single sideband phase noise at different offset frequencies ranging from 1 kHz to 1 MHz. The phase noise at 1 kHz, 10 kHz and 100 kHz are −100 dBc/Hz, −126 dBc/Hz and −135 dBc/Hz, respectively. Such results are comparable with that of mw sources based on low-noise klystrons or Gunn diodes, and fully meet the requirements of use. Table 2 displays a comparison between the phase noise of our mw source and other commonly used types of mw sources.

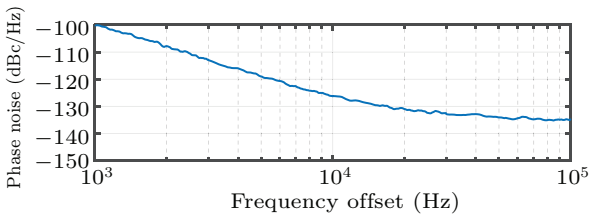


Fig. 5. Single sideband phase noise at offset frequencies ranging from 1 kHz to 100 kHz.

Table 2. Comparison between the phase noise of our mw source and others.

Type	Phase noise at 100 kHz
Klystron	−124 dBc/Hz[23]
Gunn diode (commercial)	−105 dBc/Hz
Gunn diode (cavity aided)	−145 dBc/Hz[28]
DDS	−104 dBc/Hz[29]
DDS+PDRO (ours)	−135 dBc/Hz

4.3. CW EPR experiment

The performance of our mw source in field-swept EPR experiments was examined at room temperature with a Mn^{2+} doped sample. Figure 6(a) shows the cw spectra obtained in the AFC-on (the coral solid line) and -off (the blue dash-dot line) modes, while figure 6(b) presents an enlarged detail of the first peak on the right of Fig. 6(a). In the AFC-on mode, the mw frequency keeps in resonance with the cavity, whereas in the AFC-off mode, there is a detuning of tens of kilohertz between the microwave frequency and the resonant frequency of the cavity. In each case, a sextet due to the $I = 5/2$ Mn^{2+} can be observed. However, when the AFC is switched off, the mixing of χ' and χ'' causes a serious deformation of the spectrum, rendering it top–bottom asymmetry. On the contrary, when the AFC is switched on, the deformation of the spectrum is mostly cancelled, and the cw spectrum gives more

precise information of the sample.

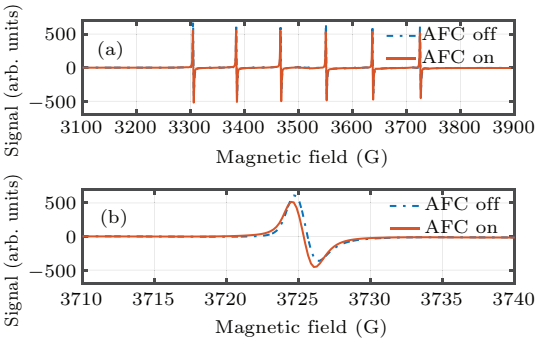


Fig. 6. (a) The overall X-band cw EPR spectra of Mn^{2+} with AFC on (the coral solid line) and off (the blue dash-dot line). (b) The enlarged detail of the first peak on the right of (a). The input mw power is 1 mW. The time constant and conversion time are both 0.02 s. The modulation amplitude and frequency of the magnetic field are 1 Gauss and 100 kHz. Each spectrum consists of 4000 data points.

5. Conclusion

We have designed an X-band mw source for EPR spectroscopy. An AFC is integrated into the mw source to track the resonant frequency of the cavity. The AFC is based on digital circuits, so its parameters can be configured flexibly depending on the experimental conditions. It is demonstrated by varying the Q factors of the cavities and the mw powers. For low phase noise, a PDRO and a DDS are utilized. A phase noise of -135 dBc/Hz at 100-kHz offset from the center frequency is achieved. The excellent performance of the mw source is also verified by cw EPR experiments, and suggests an optimistic prospect of wide applications in fields of physics, chemistry and biology.

In the future, our design can be easily extended to other wavebands by replacing the PDRO and the mixer, which ulteriorly broadens the scope of application of the mw source. The phase noise can be reduced to a much lower level with the assistance of an auxiliary cavity. Furthermore, since our mw source is highly integrated and miniaturized, it has great potential to be utilized in tabletop spectrometers.

Acknowledgements

Project supported by the Chinese Academy of Sciences (Grant Nos. XDC07000000 and GJJSTD20200001) and Hefei Comprehensive National Science Center. X. R. thanks the Youth Innovation Promotion Association of Chinese Academy of Sciences for the support.

References

[1] Zavoisky E 1946 *J. Phys.* **9** 221
[2] Cummerow R L, Halliday D and Moore G E 1947 *Phys. Rev.* **72** 1233
[3] Rana S, Chawla R, Kumar R, Singh S, Zheleva A, Dimitrova Y, Gadjeva V, Arora R, Sultana S and Sharma R K 2010 *J. Pharm. Bioall.* **2** 80
[4] Du J, Rong X, Zhao N, Wang Y, Yang J and Liu R B 2009 *Nature* **461** 1265
[5] Kempe S, Metz H and Mäder K 2010 *Eur. J. Pharm. Biopharm.* **74** 55
[6] Duss O, Yulikov M, Jeschke G and Allain F H T 2014 *Nat. Commun.* **5** 3669
[7] Song L, Liu Z, Kaur P, Esquiaquic J M, Hunter R I, Hill S, Smith G M and Fanucci G E 2016 *J. Magn. Reson.* **265** 188
[8] Crescini N, Alesini D, Braggio C, Carugno G, Gioacchino D D, Gallo C S, Gambardella U, Gatti C, Iannone G, Lamanna G, Ligi C, Lombardi A, Ortolan A, Pagano S, Pengo R, Ruoso G, Speake C C and Taffarello L 2018 *Eur. Phys. J. C* **78** 703
[9] Buckmaster H A and Dering J C 1967 *Canadian J. Phys.* **45** 107
[10] Momo F and Sotgiu A 1984 *Rev. Sci. Instrum.* **55** 253
[11] Hruszowiec M, Nowak K, Szlachetko B, Grzelczak M, Czarczynski W, Plinski E F and Wieckowski T 2017 *J. Telecommun. Inf. Technol.* **2** 18
[12] Lesniewski P and Hyde J S 1990 *Rev. Sci. Instrum.* **61** 2248
[13] Lee S H, Jou C E, Lee C P and Hu C C 1997 *Int. J. Infrared Millim. Waves* **18** 2001
[14] Pechan M J, Xu J and Johnson L D 1992 *Rev. Sci. Instrum.* **63** 3666
[15] Alecci M, McCallum S J and Lurie D J 1995 *J. Magn. Reson., Ser. A* **117** 272
[16] George A J and Teaney D T 1960 *Rev. Sci. Instrum.* **31** 997
[17] Daniels J M and Farach H A 1961 *Rev. Sci. Instrum.* **32** 1262
[18] Hyde J S and Gajdzinski J 1988 *Rev. Sci. Instrum.* **59** 1352
[19] Hirata H and Luo Z 2001 *Magn. Reson. Med.* **46** 1209
[20] Ferguson M and Mantey P 1968 *IEEE Trans. Audio Electroacoust.* **16** 392
[21] Harp M C (U.S. Patent) US3893040A [1975-07-01]
[22] Ewing G E 1976 *A digital automatic frequency control design* (Engineer's Thesis) (Monterey: Naval Postgraduate School)
[23] Edwards A V, Lasheras N C, Mcmonagle G, Arevalo M B 2021 *12th International Particle Accelerator Conference*, May 24–28, 2021, online, p. 2683
[24] Shi Z, Mu S, Qin X, Dai Y, Rong X and Du J 2018 *Rev. Sci. Instrum.* **89** 125104
[25] Eaton G R, Eaton S S, Barr D P and Weber R T 2010 *Quantitative EPR* (Vienna: Springer) pp. 25–34
[26] Feher G 1957 *Bell Syst. Tech. J.* **36** 449
[27] Lance A L, Seal W D and Labaar F 1984 *Infrared Millim. Wave* **11** 239
[28] Oles T 1992 *Rev. Sci. Instrum.* **63** 4010
[29] Li C, Lu H, Zhang X and Yuan N 2017 2017 *IEEE 2nd Advanced Information Technology, Electronic and Automation Control Conference*, March 25–26, 2017, Chongqing, China, p. 438